FR4-based electromagnetic energy harvester for wireless sensor nodes

2010 Smart Mater. Struct. 19 015022

(http://iopscience.iop.org/0964-1726/19/1/015022)

Smart Mater. Struct. **19** (2010) 015022 (11pp) doi:10.1088/0964-1726/19/1/015022

FR4-based electromagnetic energy harvester for wireless sensor nodes

G Hatipoglu and H Ürey

Electrical Engineering, Optical Microsystems Laboratory (OML), Koç University, Istanbul, Turkey

E-mail: hurey@ku.edu.tr

Received 14 June 2009, in final form 5 October 2009
Published 14 December 2009
Online at stacks.iop.org/SMS/19/015022

Abstract

Electromagnetic (EM) energy harvesting seems to be one of the most promising ways to power wireless sensors in a wireless sensor network. In this paper, FR4, the most commonly used PCB material, is utilized as a mechanical vibrating structure for EM energy harvesting for body-worn sensors and intelligent tire sensors, which involve impact loadings. FR4 can be a better material for such applications compared to silicon MEMS devices due to lower stiffness and broadband response. In order to demonstrate FR4 performance and broadband response, three moving magnet type EM generator designs are developed and investigated throughout the paper. A velocity-damped harvester simulation model is first developed, including a detailed magnetic model and the magnetic damping effects. The numerical results agree well with the experimental results. Human running acceleration at the hip area that is obtained experimentally is simulated in order to demonstrate system performance, which results in a scavenged power of about 40 μW with 15 m s^{-2} acceleration input. The designed FR4 energy scavengers with mechanical stoppers implemented are particularly well suited for nearly periodic and non-sinusoidal high-g excitations with rich harmonic content. For the intelligent tire applications, a special compact FR4 scavenger is designed that is able to withstand large shocks and vibrations due to mechanical shock stoppers built into the structure. Using our design, 0.4 mW power across a load resistance at off-resonance operation is obtained in shaker experiments. In the actual operation, the tangential accelerations as a result of the tire–road contact are estimated to supply power around 1 mW with our design, which is sufficient for powering wireless tire sensors. The normalized power density (NPD) of the designed actuators compares favorably with most actuators reported in the literature.

M This article features online multimedia enhancements

(Some figures in this article are in colour only in the electronic version)

1. Introduction

In recent years, research on harvesting useful electrical energy from the environmental vibrations has been developing rapidly. The aim is to lower dependence on the battery as a power source due to limitations like having limited lifetime and consequently needing regular replacements. One of the possible application areas of these generators is powering autonomous wireless sensor nodes such as those in intelligent tires and/or body-worn sensors.

In the literature, a majority of the power scavengers are the moving magnet type electromagnetic generators [1–5], whereas moving coil type generators are also investigated [6, 7]. Electromagnetic, piezoelectric, and other types of generators are reviewed in detail in [8–14]. Energy scavengers obtain the best performance for periodic sinusoidal excitation that matches the resonant frequency of the mechanical structure, but since the environmental vibrations are typically below 100 Hz and broadband there is a need for energy scavengers that operate at low frequencies and are broadband [15]. However, nearly all of the reported EM micro-power generators are silicon-based devices, which operate in a narrow bandwidth because of low structural damping, and at high frequencies (>kHz) due to high Young's modulus. Therefore,

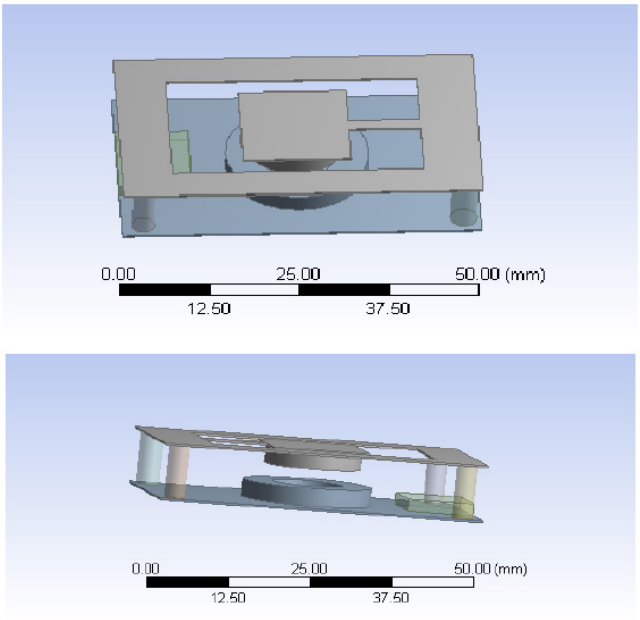

Figure 1. Schematic of energy harvester unit with FR4 cantilever. A square pad exists at the tip, on which the Nd magnet is placed. The FR4 cantilever beam carries the pad and the magnet.

these harvesters result in poor scavenging performance for most environmental vibrations. In order to improve the performance, MEMS-based-frequency up-converters are even suggested using a trap and release type interaction between a moving magnet and an array of MEMS cantilevers that carry the electromotive force (emf) coil [15]. Nevertheless, the obtained practical power was only about 4 nW. Moreover, wideband operation is tried for an acrylic cantilever beam's different modes [16].

In this work, we propose the most common printed circuit board (PCB) material, FR4 (Flame Retardant 4), as an alternative structural element that proves to be more suitable for energy harvesting applications compared to silicon MEMS devices. FR4 has a Young's modulus of 15–20 GPa (about ten times smaller than that of silicon) and is broadband due to its high intrinsic damping. FR4 is also low cost, highly integrable with electronics, and lends itself naturally to electromagnetic sensing as coils can be routed easily on the copper laminates. FR4 has been previously used as pick-up coils on copper laminates but without any mechanical functionality [2, 16]. Our group has done the pioneering work in exploring FR4 mechanical properties and its integration with electronics and micro-optics on the same movable platform [17, 18]. FR4 is a well engineered composite material for its electrical, thermal, and mechanical properties. It performed very well in reliability tests up to 250 million cycles and can be operated at stress level up to 100 MPa. For an FR4 torsional Lorentz actuator, a reliability test is run. The device is kept at slow scan resonance for about 300 million cycles. Scanner performance parameters deviated by only 10% at the end of the test run. The resonance frequency only deviated by 1%. Therefore, FR4 has already proved itself to be a good alternative to silicon MEMS devices for certain applications [17].

Table 1. Important parameters of FR4 cantilever beam system.

Parameter	Description	Value
f_n	Resonance frequency of the FR4 beam	24.8 Hz
k	Mechanical spring constant	98 N m^{-1}
Q	Mechanical Q-factor	23.36
l_b	Total beam length	10 mm
w_p	Pad width	15 mm
Nd	Magnet type	NdFeB
B_R	Magnet remanence	0.98 T
m	Magnet mass	4.036 g
R	Magnet radius	7.72 mm
h	Magnet height	3 mm
r_{ci}	Pick-up coil inner core radius	7.5 mm
r_{co}	Pick-up coil outer radius	12.2 mm
N	Number of turns	741
R_c	Coil resistance	100 Ω
R_L	Load resistance	100 Ω

The FR4 energy scavengers proposed in this paper are well suited for both low- and high-g vibration environments due to the shock stoppers built into the structure. They are particularly well suited for nearly periodic and non-sinusoidal excitations with rich harmonic content, such as those seen during human running and inside car tire surfaces.

The organization of the paper is as follows: governing equations are given for the electro-mechanical system including the magnetic damping effects in section 2. In the same section, a numerical model using Simulink® is developed that includes the magnetic damping effects to simulate the system performance for various types of inputs. In section 3, the numerical model is validated with shaker experiments. Section 4 describes a novel FR energy scavenger with shock stoppers. Section 5 details numerical and experimental results for car tire applications.

2. Governing equations and magneto-electro-mechanical system model

Figure 1 shows a schematic drawing of the simplest FR4-based energy scavenger that is developed to validate our numerical models. A cylindrical NdFeBr magnet is placed on the FR4 cantilever beam and the bobbin is placed on another non-moving FR4 board. The two boards are held together with pins. This system's parameters, that are shown in table 1, are used to validate the velocity-damped transducer simulation model developed in section 3.

The EM generator can be modeled as a spring–mass–damper system with base excitation as shown in figure 2. The relative displacement of the proof mass with respect to the base, denoted as $z(t)$, can be expressed as the difference of the proof mass displacement relative to the ground, $x(t)$, and the base displacement relative to the ground, $y(t)$,

$$z(t) = x(t) - y(t). \tag{1}$$

Then, the governing differential equation of the relative motion is given by

$$m\ddot{z}(t) + c\dot{z}(t) + kz(t) = -m\ddot{y}(t) \tag{2}$$

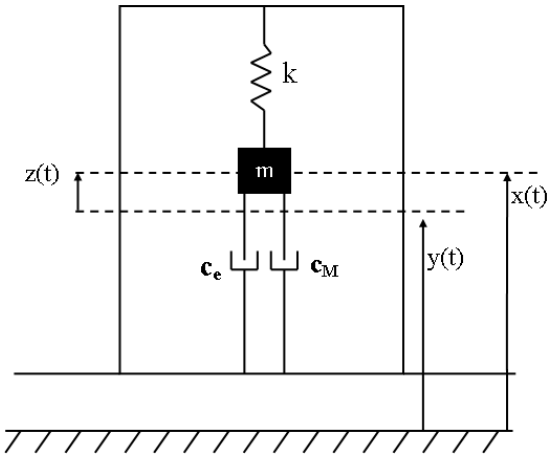

Figure 2. Linear mass–spring–damper model for inertial EM generators. k, c_e and c_M correspond to the spring constant, electrical damping coefficient and mechanical damping coefficient respectively.

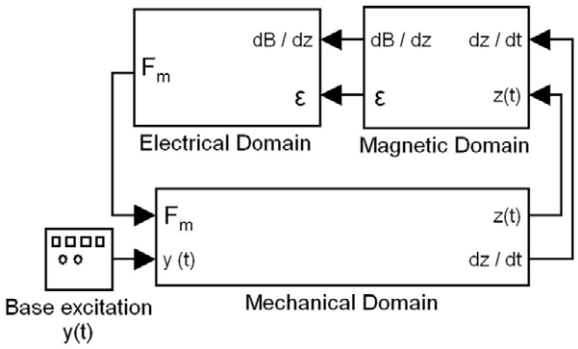

Figure 3. Matlab/Simulink system model illustrating the three coupled-energy domains.

where m is the proof mass, k is the spring constant, and c is the total damping coefficient, which includes the electrical damping and the mechanical damping.

The electrical energy extraction is generated by the relative motion of a magnet and a coil. Faraday's law of electromagnetic induction states that the time rate of change of magnetic flux (ϕ) through a coil having N turns induces a voltage (emf) given by

$$\varepsilon = -N\frac{\mathrm{d}\phi}{\mathrm{d}t} \qquad \text{where } \phi = \int_A \vec{B}\cdot\mathrm{d}\vec{A} \tag{3}$$

where $\vec{B}$ is the magnetic flux density. Equation (3) can be simplified by assuming A is constant for small displacements and the area vector stays parallel to the magnetic flux direction [19]:

$$\varepsilon = -NA\frac{\mathrm{d}B}{\mathrm{d}z}\frac{\mathrm{d}z}{\mathrm{d}t} = -NA\frac{\mathrm{d}B}{\mathrm{d}z}\dot{z}(t). \tag{4}$$

If the pick-up coil terminals are left open (i.e. open-loop operation), then the above expression is valid. If an induced current is generated by the presence of a load such as a capacitor or a battery to store the energy, then the system is in closed-loop mode and there is an additional magnetic damping term generated by the induced current $i(t)$, which effectively counteracts the motion of the magnet. This magnetic damping force (F_M) can be expressed as [20]

$$F_M = NA\frac{\mathrm{d}B}{\mathrm{d}z}i(t). \tag{5}$$

A numerical simulation model is developed using equations (2), (4), and (5).

2.1. Numerical model overview

The total energy harvester physical system consists of three coupled-energy domains as shown in figure 3. The system is modeled in a Matlab/Simulink environment and can handle both open-loop and closed-loop operation.

The base excitation is the acceleration input to the system due to environmental vibrations. Sinusoidal and non-sinusoidal nearly periodic inputs such as those generated with human running and a car tire are tested with the model. The parameter $\mathrm{d}B/\mathrm{d}z$ is a critical input to the system. It is obtained using finite element modeling (FEM) simulations and a polynomial fit is obtained in Matlab™ by the least squares method for the numerical simulations (explained in more detail in section 2.2). The model solves for the magnet displacement, induced emf and induced current assuming R_c and R_L. For open-loop operation, the induced current and back-emf are zero and the solution is much simpler. Figure 4 shows the overall model.

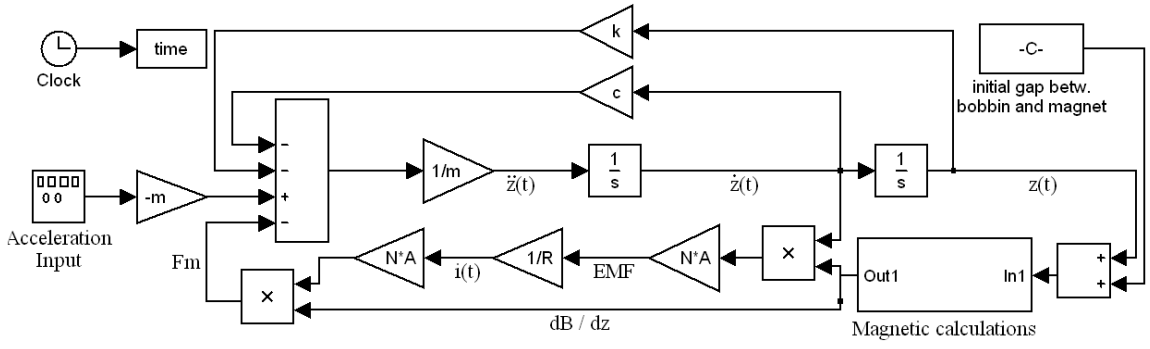

Figure 4. The Matlab/Simulink Model. The 'magnetic calculations' subsystem is explained in section 2.2 in detail.

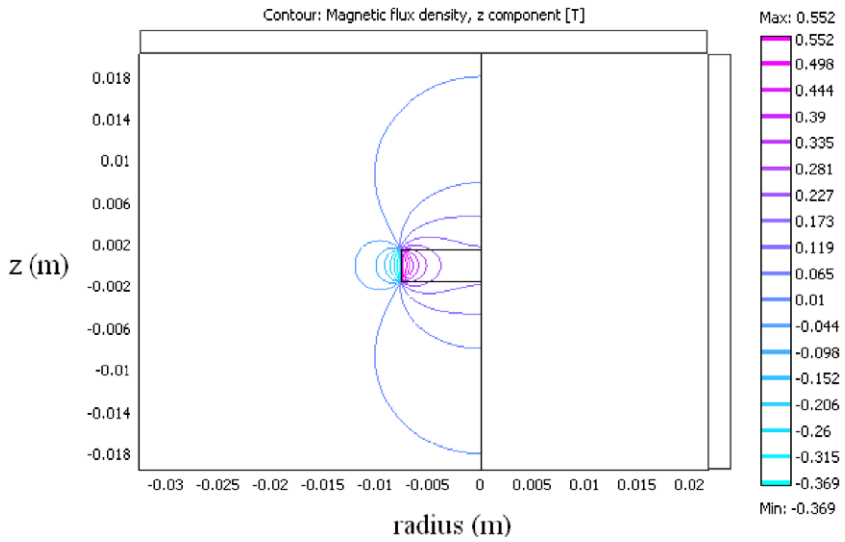

Figure 5. 2D axis-symmetric magnetic flux density distribution of the magnet used in the FR4 case study. If the figure is rotated by 360° about the symmetry axis, the 3D distribution of the magnetic flux density may be obtained [22].

2.2. System magnetic model

As a case study, the FR4 cantilever system shown in figure 1 and the corresponding parameters shown in table 1 are used to implement the electromagnetic domain parameters into the transducer simulation model. The only unknown parameter in equations (4) and (5) is $\mathrm{d}B/\mathrm{d}z$, which is obtained using a lengthy procedure as explained below and makes an important contribution to modeling the magnetic field effects in electromagnetic harvesters.

For a generic cylindrical magnet as defined in table 1, the magnetic flux density, B, along the axis of its centerline as a function of distance z from the pole surface is given by [21]

$$B(z, r = 0) = \frac{B_r}{2}\left(\frac{(h+z)}{\sqrt{R^2+(h+z)^2}} - \frac{z}{\sqrt{R^2+z^2}}\right). \quad (6)$$

The formula above is first validated by obtaining magnetic flux density, B, along the axis of magnet centerline experimentally using a teslameter (model Magnet-Physik F54) and a micrometer stage. Then, a B_r value is obtained from this experiment. This value is just used to model the magnet's magnetization in FEM precisely. The centerline distribution itself is not enough, so numerical simulations are needed in order to obtain an expression for the distribution of magnetic flux density, B, across the area enclosed by the pick-up coil, A. Due to the cylindrical magnet geometry, a 2D axis-symmetric magnetostatic analysis is performed in COMSOL Multiphysics. B distribution over A is extracted from the analysis via small z increments. Figure 5 illustrates B as a function of r and z. These magnetic flux density values corresponding to each z are averaged. The obtained average magnetic flux density change over A, as a function of z values, is shown in figure 6. A mathematical fit function is then utilized for $B(z)$. Later, $\mathrm{d}B/\mathrm{d}z$ is computed in Matlab and the resultant exponential fit function is used in the magnetic calculations subsystem in Simulink®. A third order exponential function,

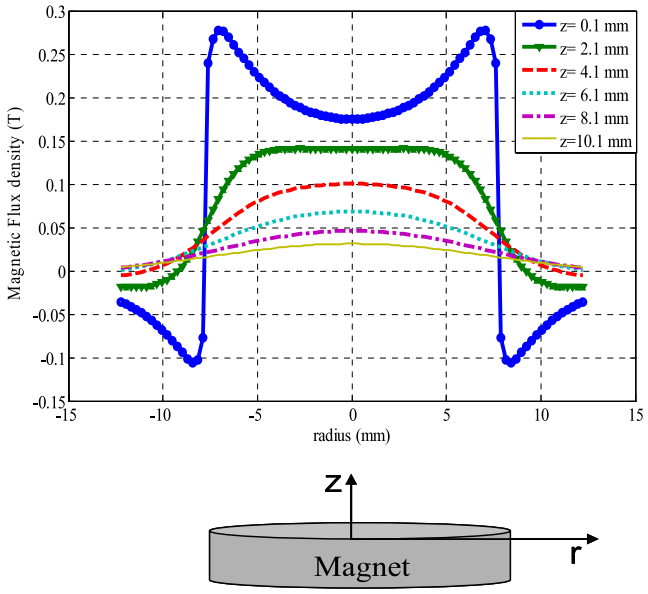

Figure 6. Magnetic flux density z component over the pick-up coil (table 1) enclosed area at various z distances from the magnet pole surface.

which is expressed with equation (7), fit well to these values, given as

$$B(z) = \mathrm{e}^{Az^3+Bz^2+Cz+D}. \quad (7)$$

The constants A, B, C, and D in the equation are calculated in Matlab by the least squares method and used in the magnetic subsystem model in figure 4. Figure 7 illustrates the resultant $B(z)$ and $\mathrm{d}B/\mathrm{d}z$ for the geometry in figure 1 whose parameters are shown in table 1.

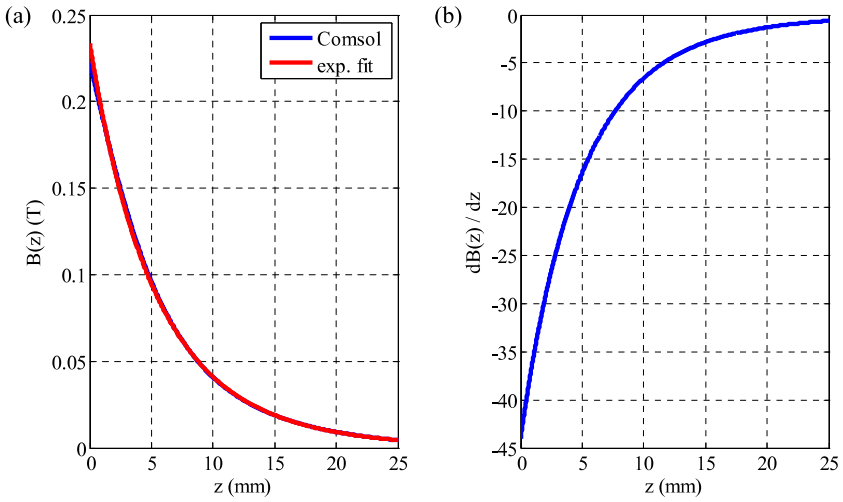

Figure 7. (a) Average magnetic flux density distribution ($B(z)$) over the bobbin area, A, versus distance from the magnet pole surface, z. (b) Position rate of change of magnetic flux density, $\mathrm{d}B/\mathrm{d}z$, versus distance from the magnet pole surface.

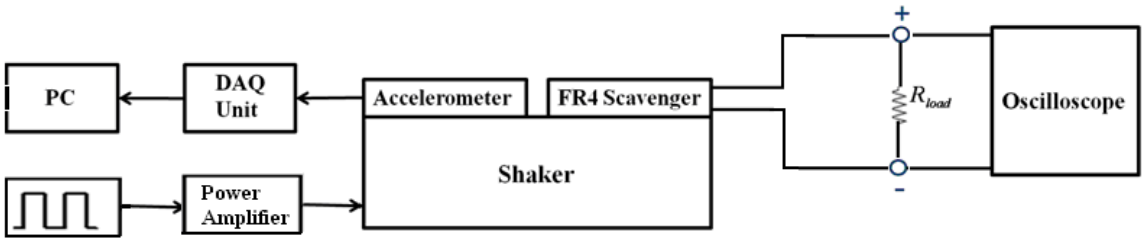

Figure 8. Experimental setup for the shaker experiments using R_{L}.

3. Model validation with shaker experiments

In order to test and validate the simulation model and observe the performance of the FR4 cantilever, shaker experiments are carried out. The schematic setup is shown in figure 8.

3.1. Square-wave base excitation results

The simulation model is first validated with the FR4 cantilever shown in figure 1. The FR4 energy harvester is tested with a 50% duty cycle pulse acceleration with ± 15 m s^{-2} peak acceleration. A frequency sweep is performed. Figure 9 compares the simulation and experimental results on induced voltages as a function of excitations below the harvester resonance frequency as a result of pulse input for closed-loop (with magnetic damping) and open-loop operations (without magnetic damping). Around 22 Hz (near the 24.8 Hz resonance), the sample plastically deformed and nearly failed and the experiment was stopped.

Despite a large number of variants in mechanics and magnetics, the model agrees well with the experiments for both open-loop and closed-loop cases. The local extrema of emf are obtained when the harmonics of the excitation frequency coincide with the mechanical resonance (i.e., $f_{\mathrm{e}} = f_{\mathrm{n}}/3$, $f_{\mathrm{n}}/5$, etc). For each such f_{e}, the mechanical oscillations are at f_{n}. The FR4 cantilever is designed to have a resonant frequency of 24.8 Hz, which results in maximum emf output. It is difficult to

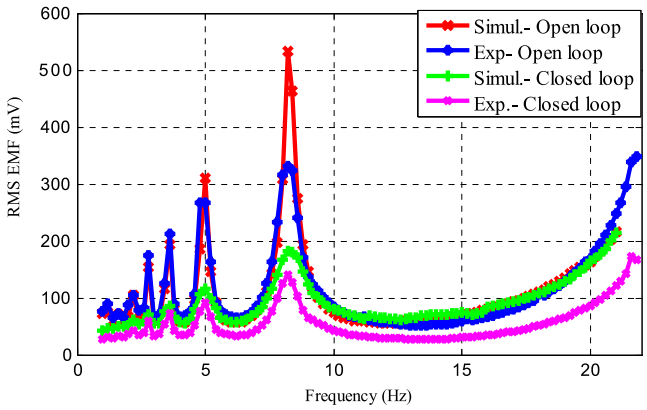

Figure 9. Frequency response of the system for a square-wave excitation at frequencies below the mechanical resonance of 24.4 Hz using the FR4 cantilever shown in figure 1.

design feasible structures with silicon at such low frequencies due to cost and shock-vibration survivability factors. Notice that each peak is fairly broad. Since our applications involve impact loadings, the energy at harmonics of the excitation is much higher than the fundamental frequency of the vibration. Therefore, the broadband operation is possible by selecting a mechanical resonant frequency where there is sufficient energy for a broad range of excitation frequencies. The tested FR4 sample is almost broken close to resonance during the

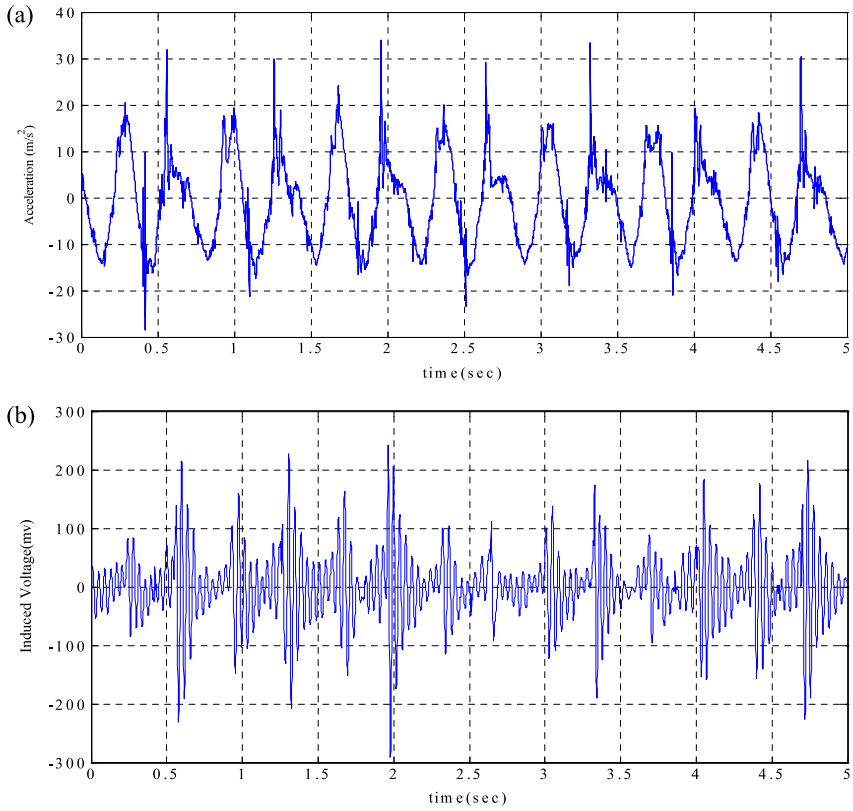

Figure 10. (a) Acceleration waveform obtained from a running test subject at the hip area; (b) corresponding emf predicted by the simulation model.

experiments for the indicated input; therefore, the data reported in figure 9 are limited to 22 Hz. Therefore, the mechanical stopper mechanism, which is explained in sections 4 and 5, is incorporated into the FR4 design to mainly reduce the stress on flexures.

3.2. Excitation with human running experimental data

One of our application areas is body-worn wireless sensors. Human running motion is, therefore, investigated as an exemplary body motion. The pulse excitation in section 3.1 is chosen to mimic the acceleration data obtained using running human subjects, illustrated in figure 10(a), where each stride waveform is like a short pulse. The accelerometer is connected to the hip area of human subjects while acquiring the data experimentally. Figure 10(b) demonstrates the predicted induced emf for the FR4 cantilever for the acceleration input obtained from a human subject. The simulations predict 39.5 μW rms power over R_L for the given input at 2.75 Hz average stride frequency. The experiment is repeated with three male subjects. The stride frequencies and the anticipated emf results are similar. In the experiment performed with square-wave base excitation in section 3.1, the obtained rms power at 2.75 Hz input is 34 μW (figure 9). The close power levels also prove that each stride is like an impulse to the scavenging system, which can be crudely approximated with a short pulse.

Since our numerical model works well, all other types of inputs can be evaluated with the same model for any inertial energy harvester including MEMS-based devices. Thus, evaluation of the system performance and optimization can be easily executed.

4. Compact FR4 design for high-*g* acceleration environments

Figure 11 shows the compact EM scavenger geometry and the novel FR4 spring design. It is designed to achieve higher power density and good shock survivability. The springs are hidden underneath the magnet and the volume of the device is determined essentially by the pick-up coil and the oversized magnet, which is placed on top of the FR4 spring with a spacer.

When compared with the initial macro FR4 cantilever design of figure 1, the practical volume is reduced by 74% down to 4.1 cm^3 while a bigger Nd magnet ($B_r = 0.98$ T) having 6.5 mm radius, 6 mm height, and 5.36 g of weight is used that generates more power. The spacer limits the maximum allowable deflections of the magnet in one direction and prevents failure of the springs due to high-g shocks. In the other direction, the bobbin acts as a mechanical stopper. At large displacements, actuator flexures make contact with the bobbin and the spacer. The schematic view of all components of the system is shown in figure 12. The spacer stays completely inside the pick-up coil, which is attached to both the magnet and to the clear aperture of the actuator. Since the mechanical stoppers limit the deflection of the FR4 spring to about ± 1 mm, the vibration amplitude is reduced enforcedly. Some of the magnet's kinetic energy is lost during these hard

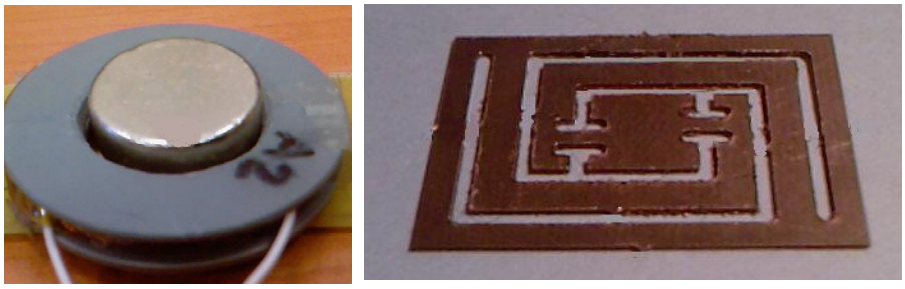

(a) (b)

Figure 11. (a) Assembled FR4 energy scavenger design with spacers. (b) The unique actuator design having total dimensions of 20 mm × 16 mm × 0.178 mm. It is completely hidden under the oversized magnet.

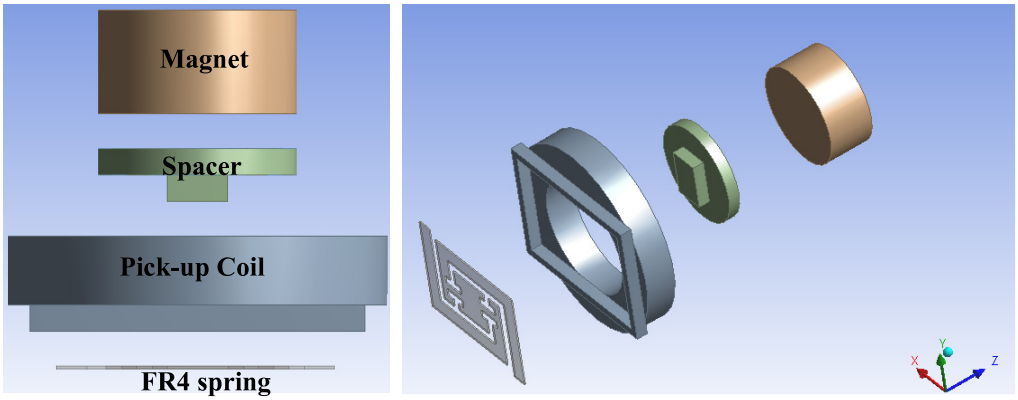

(a) (b)

Figure 12. (a) Components of the scavenger unit. (b) The FR4 actuator is glued on the FR4 platform that is attached to the pick-up coil (bobbin). The bobbin acts as a mechanical stopper in the $+z$ direction whereas the stopper is the spacer itself in the $-z$ direction.

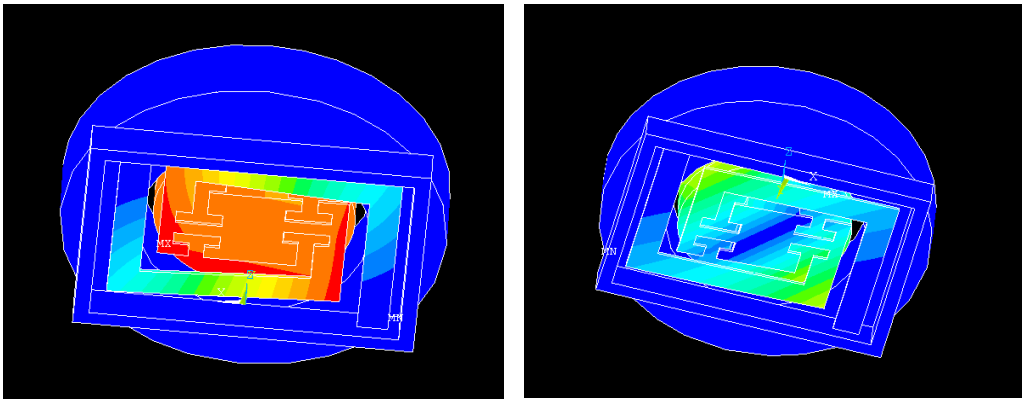

(a) (b)

Figure 13. The backside of the compact FR4 harvester showing the spring modes: (a) out of plane mode at 24.4 Hz; (b) torsion mode at 14.4 Hz.

contacts and the harvester becomes less efficient. However, in high acceleration environments, sufficient power can be obtained without exceeding the elastic deformation limits of the springs. This is discussed in more detail in section 5.1.

The actuator geometry is chosen to have a spiral shape. The spiral spring design offers the following advantages: (i) it allows for low spring constant and energy harvesting for both torsion and out-of-plane vibration modes at 14.4 Hz and 24.4 Hz, respectively (see figure 13); (ii) it can be hidden underneath the magnet using a spacer, allowing for a more compact actuator that fits tightly inside the pick-up coil; (iii) the spacer, which is placed on the moving central platform, separates the spiral spring and the larger magnet. It also acts as a mechanical stopper to limit stress on the springs. Owing to the spiral spring design and the spacer, the magnet (5.4 g) is heavier than the cantilever design magnet (4 g), which creates larger actuation forces, improving the power density.

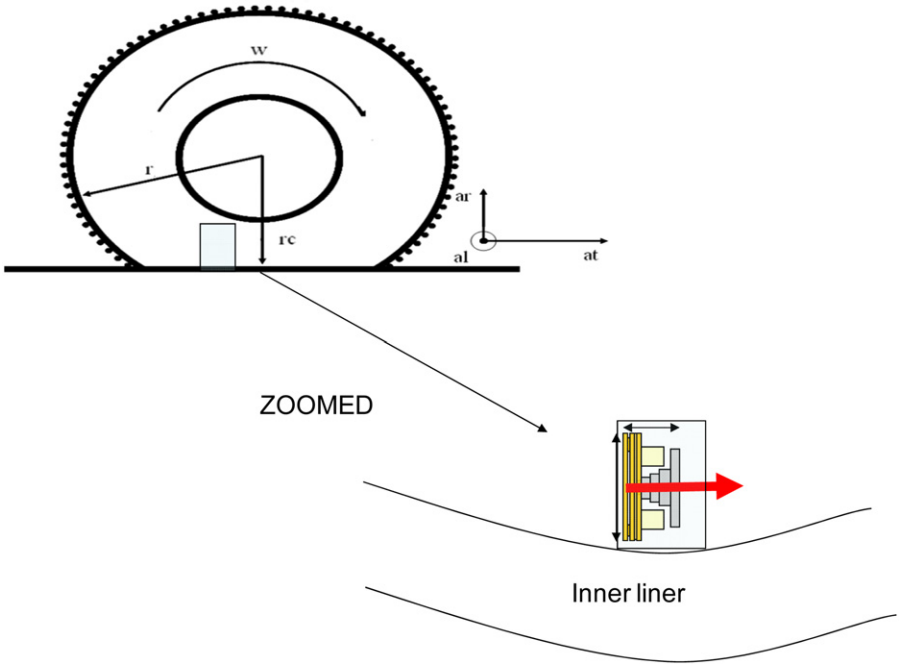

Figure 14. The planned mounting of the harvester for tire applications is demonstrated. In this configuration, a_t favors out of plane deflection while torsional deflections are favored by a_r. The red arrow shows the out of plane deflection direction due to tangential acceleration. The figures are not drawn with actual scales and the deflection of the tire is exaggerated.

The shaker experiments described in section 3.1 are repeated for this device. It is observed that the compact design with spacers is more efficient than the cantilever-based design. For comparison, using the same coil and pulse excitation at the mean human running frequency of 2.75 Hz, the compact FR4 design with spacer generates 49 μW rms power, which is an improvement of 25% compared to the cantilever-based design of figure 1.

The FR4 energy scavenger is also tested with a 2 m s^{-2} sinusoidal peak-to-peak acceleration at the device resonant frequency of 24.4 Hz and compared with the reported scavengers in the literature [23]. An rms power of 0.144 mW is obtained using a standard load resistance of $R_L = 100\ \Omega$. Despite not being fully optimized, it demonstrates a notable normalized power density (NPD) of 35.1 kg m^{-3}. Some of the better NPD values are obtained for higher resonant frequency devices and using vacuum conditions. However, low frequency devices are more efficient energy harvesters for the applications mentioned in this paper. Likewise, vacuum conditions create sharp resonances but environmental vibrations are typically broadband and non-sinusoidal. Therefore, NPD measured at resonant frequency is not a very good metric for practical applications involving broadband environmental vibrations, but it is a good scale to compare the harvester performance of various devices.

5. Tire sensor application case study

5.1. Tire–road interaction

After testing with short pulse excitation and human running input as examples of impact excitation, powering tire sensors is studied as a case study for FR4-based energy harvesters. In order to avoid battery change during the life of a tire, there is a need for a broadband and robust scavenger for the wireless intelligent sensors, which are vitally used in tire applications like the Pirelli Cyber™ Wheel [24] and SmarTire Systems [25] in order to monitor the tire–road interaction or tire condition and even to track the internal air pressure of the tire. While the tire rotates, a region of the tire contacts with the road periodically. During this cyclic deformation, accelerations occur in three different directions, which are lateral (a_l), tangential (a_t) and radial (a_r) due to rotation and deflection of the tire. As illustrated in figure 14, the contact region of a tire elastically deforms and becomes almost flat due to the weight of a vehicle. In our work, the target is to harvest energy by mainly utilizing the tangential accelerations, which are impacts resulting from the tire–road contact and present even at constant vehicle speeds. The tire deformation due to contact supplies tangential acceleration amplitudes reaching up to 300 g depending on the tire operating conditions [26].

An example of the expected tangential acceleration waveform due to contact deformation, occurring for a vehicle having a translational speed of 30 kph, resulting in 4.65 Hz periodic excitation considering the tire scavenging system is placed along the inner liner of a 195/50 R15 tire, is demonstrated in figure 15. The acceleration waveforms fit analytically very well with the first derivative of a Gaussian function and the contact duty cycle is estimated at 10–15%. For example, the magnitude and the shape of the waveform shown in figure 15 fit well with the first derivative of a Gaussian pulse having an equation such as

$$a(t) = 0.18 \exp(-(T/2 - t)^2/2\sigma^2) \qquad (8)$$

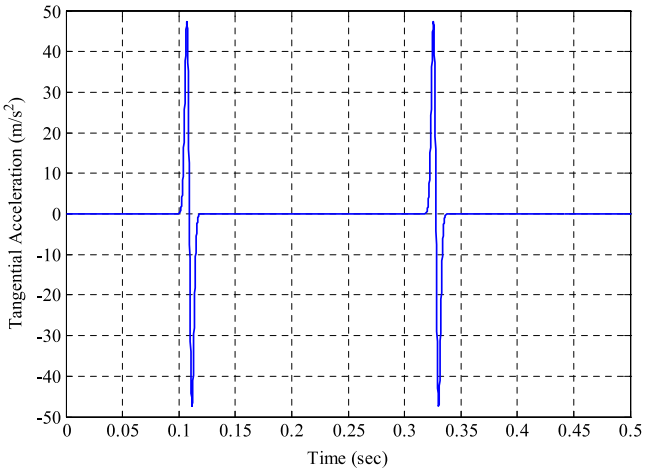

Figure 15. The expected tangential accelerations due to tire–road contact for a translational speed of 30 kph for a vehicle having a 195/50 R15 tire [26].

Figure 17. Tire energy harvesters. The Nd oversized magnet has a radius of 10 mm and a height of 2 mm. Four smaller Nd magnets are placed under the bigger magnet, acting as spacers, enabling us to place the oversized magnet on top.

where T is the period ($T = 0.215$ s for 30 kph) and σ is the variable determining the duty cycle ($\sigma = 0.0023$ for 30 kph).

The rotational speed of the tire and the impact frequency scales linearly with the vehicle speed, whereas expected acceleration values are proportional to squared speeds [26]. In order to design the tire energy harvester at optimum levels, the frequency spectra for different wheel translational speeds are obtained. Figure 16 demonstrates the frequency spectra of the tangential accelerations occurring as a result of tire–road contact. The waveforms have rich harmonic content, increasing the power harvesting efficiency of our system at off-resonance operation. The harvester mounting and wiring conditions depend on application and are not detailed here. The harvester orientation for the design considered here should favor tangential acceleration and out-of-plane deflections. Due to the coupling of different modes and acceleration components during the contact time, the torsion mode is also excited, increasing the harvester performance.

5.2. FR4-based tire energy harvester

The sensor illustrated in figure 17 is designed for the tire scavenger application and it has 46 Hz resonant frequency.

The resonance frequency of the tire energy harvester is set according to the harmonic distribution of possible vehicle speeds. Since the tire experiences high amplitude accelerations during the rotation, the spacer mechanism explained in section 4 is again incorporated into the system. However, four smaller Nd stacked magnets beneath one oversized Nd magnet ($B_r \approx 1$ T) on the top are utilized as spacers rather than using FR4 as a spacer. A schematic of the stacked magnet and FR4 platform assembly is shown explicitly in figure 18. The smaller magnets completely stay inside the pick-up coil, enabling us to achieve a more compact design while increasing the flux density gradient.

In order to test tire scavenger performance, shaker experiments are performed for various vehicle speeds. The desired tire–road contact tangential acceleration waveforms similar to those shown in figure 15 are given by the shaker over an arbitrary signal generator. Since the shaker is driven

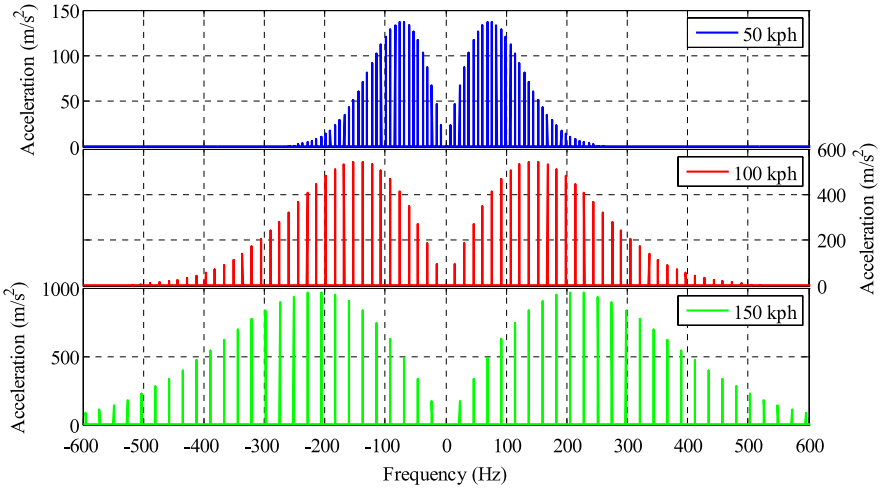

Figure 16. The frequency spectra of expected tangential accelerations occurring at selected translational vehicle speeds.

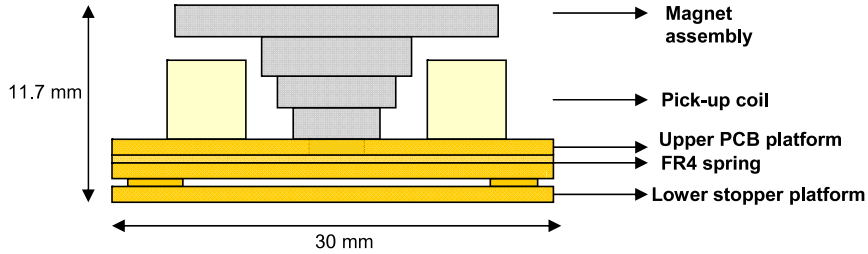

Figure 18. The FR4 spring, having a very similar design to the spring shown in figure 11(b), is sandwiched between two thicker FR4 platforms. This time, the oversized magnet, lower stopper platform and bobbin act as mechanical stoppers.

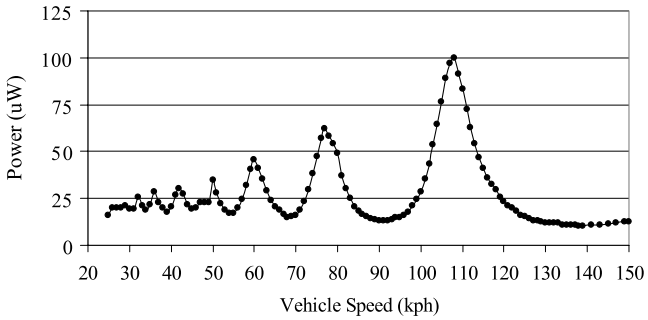

Figure 19. Power across R_L versus various vehicle speeds for 3 g p–p tangential acceleration input. Corresponding contact frequencies can be calculated using the conversion factor 1 Hz = 6.57 kph.

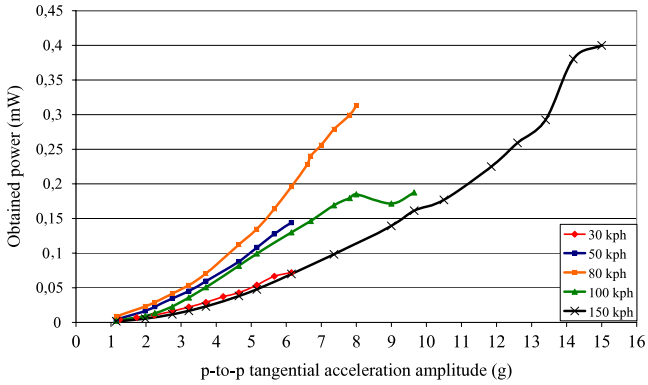

Figure 20. Power across $R_L = 100\ \Omega$ versus increasing acceleration amplitude for five different vehicle speeds.

with displacement data, the integral of the Gaussian function, which is the error function, is fed to the shaker to obtain the desired shaped acceleration waveforms. The acceleration input is fixed at constant amplitude, that is 1.5 g. In actual operation, the amplitudes are increasing as the vehicle speed increases. However, the high acceleration values could not be achieved by the shaker at low frequencies due to shaker frequency–amplitude limitations. Figure 19 exhibits the tire energy harvester's wideband response to acceleration inputs for different speeds (contact frequencies). As the harmonics of the device matching with the excitation frequency, local peaks in the power are observed. Since the Q value of the structure is low, unlike silicon-based energy harvesters, the power output is broadband. Therefore, electrical induction is not limited just to resonance operation. Indeed, it is extended to off-resonance operation.

In order to estimate the power output in actual operation, a final shaker experiment is carried out. For five different vehicle speeds, tangential acceleration amplitude is increased to the limits of the shaker for each frequency. Since the shaker can give higher amplitudes at higher frequencies, the acceleration amplitudes are increased during testing of the tire energy harvester. As shown in figure 20, the tire energy harvester can generate 0.4 mW power across R_L at off-resonance operation for 15 g p-to-p tangential acceleration input corresponding to 150 kph speed. Considering the fact that 150 kph vehicle speed is a local minimum at power generation (figure 19), the power levels at coinciding harmonics for a single device could easily go up to the 1 mW range, which is sufficient to power wireless tire sensors. Multiple FR4 scavengers can be connected in series to increase the power further. Furthermore, the single device is tested for 10.8 m s^{-2} acceleration input amplitude at its resonance operation; it exhibits an rms power of 0.876 mW across R_L.

6. Conclusions

For energy harvesting applications, wideband electrical energy production is a more desirable method since environmental vibrations are also broadband. As in the cases of human running motion and tire–road contact, the excitations may be impacts with rich harmonic content. In addition to resonance operation, energy harvesting at harmonics is an efficient way to increase the harvesting frequency range of devices. When compared to silicon-based MEMS devices, FR4 has very low Q values, which let FR4 actuators we have developed operate in broadband. Also, FR4 proves to be a more suitable material to design low frequency and robust energy harvesters. For tire scavenging applications, about 0.3 mW is obtained assuming an acceleration of 8 g at 80 kph using tangential accelerations. In reality, peak tangential acceleration at such vehicle speeds are about 35 g and the scavenged power should be easily above 1 mW.

The introduced spacer mechanism increases the power density as well as the robustness of the harvesting devices. At high amplitude inputs, hard mechanical contacts occur, which may cause fatigue failure. FR4 reliability has been tested before by our group. FR4 did not show any degradation in performance during cyclic stress tests up to about 100 MPa

stress levels for several million cycles. Since the fatigue stress of FR4 is around 100 MPa, all of our devices are designed according to this stress value. Moreover, the maximum ultimate tensile strength (UTS) of copper laminated FR4 is around 370 MPa. The ratio of fatigue strength to UTS is 27%. Furthermore, copper around FR4 is ductile. Surface crack propagation has less chance to occur compared to a brittle material. It has many advantages from a durability perspective. However, more detailed research is going on in order to increase our knowledge about impact fatigue at the moment. Our next step is to determine the contact strength and life of FR4 and optimize the FR4 utilization as a promising alternative to MEMS devices for electromagnetic power harvesters.

Acknowledgments

The authors are grateful to Dr Erdem Alaca for his support during the research. We would like to thank Dr Ipek Basdogan for providing access to the shaker and Utku Baran and Adil Tolga Gorgulu for helping to carry out shaker experiments. Also, we thank Selim Olcer for his effort on manufacturing the FR4 actuators in our facilities. This work is accomplished by a Tubitak fellowship to GH and a TUBA-GEBIP grant to HÜ.

References

[1] El-Hami M, Glynne-Jones P, James E, Beeby S P, White N M, Brown A D, Ross J N and Hill M 2001 Design and fabrication of a new vibration-based electromechanical power generator *Sensors Actuators* A **92** 335–42

[2] Ching N N H, Chan G M H, Li W J, Wong H Y and Leong P H W 2000 PCB integrated micro-generator for wireless systems *Proc. Int. Symp. Smart Structures and Microsystems (Hong Kong)*

[3] Ching N N H, Wong H Y, Li W J, Leong P H W and Wen Z 2001 A laser-micromachined multi-modal resonating power transducer for wireless sensing systems *Sensors Actuators* A **97/98** 685–90

[4] Glynne-Jones P, Tudor M J, Beeby S P and White N M 2004 An electromagnetic, vibration-powered generator for intelligent sensor systems *Sensors Actuators* A **110** 344–9

[5] Yuen S C, Lee J M, Li W J and Leong P H 2007 An AA-sized vibration-based microgenerator for wireless sensors *IEEE Pervasive Comput.* **6** 64–72

[6] Amirtharajah R and Chandrakasan A P 1998 Self-powered signal processing using vibration-based power generation *IEEE J. Solid-State Circuits* **33** 687–95

[7] Beeby S P, Tudor M J, Koukharenko E, White N M, O'Donnell T, Saha C, Kulkarni S and Roy S 2005 Micromachined silicon generator for harvesting power from vibration *Proc. Transducers 2005 (Seoul)* pp 780–3

[8] Beeby S P, Tudor M J and White N M 2006 Energy harvesting vibration sources for microsystems applications *Meas. Sci. Technol.* **17** 175–95

[9] Anton S R and Sodano H A 2008 A review of power harvesting using piezoelectric materials (2003–2006) *Smart Mater. Struct.* **16** 1–21

[10] Williams C W, Woods R C and Yates R B 1996 Feasibility study of a vibration powered micro-electric generator *IEE Colloquium on Compact Power Sources (London)* pp 7/1–7/3

[11] Sodano H A, Lloyd J and Inman D J 2006 An experimental comparison between several active composite actuators for power generation *Smart Mater. Struct.* **15** 1211–6

[12] Renaud M, Fiorini P, Shaijk R and Hoof C 2009 Harvesting energy from the motion of human limbs: the design and analysis of an impact-based piezoelectric generator *Smart Mater. Struct.* **18** 1–16

[13] Mitcheson P D, Miao P, Stark B H, Yeatman E M, Holmes A S and Green T C 2004 MEMS electrostatic micro-power generator for low frequency operation *Sensors Actuators* A **115** 523–9

[14] Meninger S, Mur-Miranda J O, Amirtharajah R, Chandrakasan A P and Lang J H 2001 Vibration-to-electric energy conversion *IEEE Trans. Very Large Scale Integr. (VLSI) Syst.* **9** 64–76

[15] Kulah H and Najafi K 2004 An electromagnetic micro power generator for low-frequency environmental vibrations *Micro Electro Mechanical Systems—17th IEEE Conf. On MEMS (Maastricht)* pp 237–40

[16] Yang B, Lee C, Xiang W, Xie J, He J H, Kotlanka R K, Low S P and Feng H 2009 Electromagnetic energy harvesting from vibrations of multiple frequencies *J. Micromech. Microeng.* **19** 035001

[17] Urey H, Holmstrom S and Yalcinkaya A D 2009 Electromagnetically Actuated FR4 Scanners *IEEE Photon. Technol. Lett.* **20** 30–2

[18] Isikman S O, Sprague R B and Urey H 2009 FR4 laser scanner with dynamic focus *IEEE Photon. Technol. Lett.* **21** 233–5

[19] Mitcheson P D, Green T C, Yeatman E M and Holmes A S 2004 Architectures for vibration-driven micropower generators *IEEE J. Microelectomech. Syst.* **13** 429–40

[20] Buren T and Troster G 2007 Design and optimization of a linear vibration-driven electromagnetic micro-power generator *Sensors Actuators* A **135** 765–75

[21] Zhang T, Jiang C, Xu H and Mao J 2007 Permanent-magnet longitudinal fields for magnetostrictive devices *J. Appl. Phys.* **101** 034511

[22] Spreemann D, Hoffmann D, Folkmer B, Maurath D and Manoli Y 2007 Advanced numerical modeling of electromagnetic vibration transducer under realistic condition *PowerMEMS (Freiburg)* pp 97–100

[23] Beeby S P, Torah R N, Tudor M J, Glynne-Jones P, O'Donnell T, Saha C R and Roy S 2007 A micro electromagnetic generator for vibration energy harvesting *J. Micromech. Microeng.* **7** 1257–65

[24] Pirelli Tire: United States. Pirelli-Cyber™ Wheel. US: Pirelli & C. S.p.A.; [Updated 2006 July 14; cited 2009 June 14] Available from: http://www.us.pirelli.com/web/technology/technology-revolution/cyber-wheel/default.page

[25] Bendix CVS Canada Inc. SmarTire Systems. Richmond, BC, Canada: Bendix Commercial Vehicle Systems LLC. [Cited 2009 June 14] Available from: http://www.smartire.com/

[26] APOLLO Intelligent tyre for accident-free traffic 2001 *Technical Research Centre of Finland (VTT)* p.IST-2001-34372